Journal Name

ARTICLE TYPE

Cite this: DOI: 10.1039/xxxxxxxxxx

# First-principles study of structural stability and electro-chemical properties of $Na_2MSiO_4$ *M* = Mn, Fe, Co and Ni) polymorphs†

F. Bianchini,*[a] H. Fjellvåg,[a] and P. Vajeeston[a]

Received Date
Accepted Date

DOI: 10.1039/xxxxxxxxxx

www.rsc.org/journalname

Sodium orthosilicates $Na_2MSiO_4$ ($M$ = Mn, Fe, Co and Ni) have attracted much attention due to the possibility of extraction two Na ions per formula unit. They are also found to exhibit a great structural stability due to a diamond-like arrangement of tetrahedral groups. In this work we have systematically studied the possible polymorphism of these compounds by means of density functional theory, optimising the structure of a number of systems with different group symmetries. The ground state is found to be Pc-symmetric for all the considered $M$ = Mn, Fe, Co, Ni, and several similar structures exhibiting different symmetries coexist within a 0.3 eV energy window from this structural minimum. The intercalation/deintercalation potential is calculated for varying transition metal atoms $M$. Iron sodium orthosilicates, attractive due to the natural abundance of both materials, exhibit a low voltage, which can be enhanced by doping with nickel. The diffusion pathways for Na atoms are discussed, and the relevant barriers are calculated using the Nudged Elastic Band method on top of DFT calculations. Also in this case nickel impurities would improve the material performances, by lowering the barrier heights. Notably, the ionic conductivity is found to be systematically larger with respect to the case of lithium orthosilicates, due to a larger spacing between atomic layers and to the non-directional bonding between Na and the neighbouring atoms. Overall, the great structural stability of the material together with the low barriers for Na diffusion indicates this class of materials as a good candidate for modern battery technologies.

In recent years Na-ion batteries are attracting increasing interest from the scientific community. They are considered the most attractive alternative to Li-ion batteries, due to the low cost and widespread abundance of sodium. Electrode materials research is following a strategy analogous to the Li-ion case, investigating the structural and diffusive properties of layered oxides[1], phosphates[2] and titanates.[3] The family of intermetallic lithium orthosilicates $Li_2MSiO_4$, where $M$ = Mn, Fe, Co, and Ni, has been the focus of several studies,[4–9] due to the possibility of exchanging two electrons per formula unit corresponds to theoretical capacities in excess of 300 mA h $g^{-1}$.[7] However, this process is difficult to achieve and most experimental work report the extraction of only one ion.[7] Furthermore, these materials exhibit a complex and rich polymorphism,[9,10] and a phase transition is known to occur upon battery cycling, significantly decreasing the initial capacity of $Li_2FeSiO_4$.[4]

More recently, $Na_2MSiO_4$ compounds are recognised as more promising candidates for novel cathode materials.[11–15] It has been inferred by means of *ab initio* calculations that full extraction of Na ions is easier to achieve with respect to the case of lithium due to a lower deintercalation voltage plateau.[16] Furthermore, the diffusion barrier for Na ions is found to be significantly lower. This trend is preserved for different structural phases[16,17] and can be attributed to the larger equilibrium volumes predicted for Na-based compounds, which corresponds to a weaker interac-

[a] *Department of Chemistry University of Oslo, Box 1033 Blindern, N-0315 Oslo, Norway*
* *E-mail federico.bianchini@smn.uio.no*
† Electronic Supplementary Information (ESI) available. See DOI: 10.1039/b000000x/

tion between atomic layers with respect to the case of lithium orthosilicates. Notably, Na doping would improve the performance of a Li-based cathode due to this feature.[16] Na-based orthosilicates are also known to exhibit a greater structural stability upon cycling with respect to their lithium counterparts,[15,18] due to the high Na/Fe exchange barriers observed for equilibrium structures exhibiting a diamond-like arrangement of $AO_4$ ($A$ = Fe, Si) tetrahedral blocks.[12] DFT studies of these structures report also a very small volume change (below 3%) upon complete desodiation.[12] Experimental studies are overall in agreement with the predicted structural stability,[15,18,19] observed only when control over impurities is achieved[14]. In 2011, Duncan and coworkers first successfully synthesised $Na_2MnSiO_4$ (space group Pc) using a sol-gel method.[20] Chen and coworkers synthesised $Na_2MnSiO_4$ following the same procedure, and measured a reversible capacity of 125 mA h $g^{-1}$, which is the first evaluation of electrochemical properties for Na-based orthosilicate cathodes.[11] More recently, $Na_2CoSiO_4$, prepared via hydrothermal method, was used as positive electrode material for Na-based capacitors[18] and sodium iron orthosilicate $Na_2FeSiO_4$ was synthesized and reported to exhibit reversible electrochemical activity of 106 mA h $g^{-1}$.[15] The latter material is particularly attractive due to the natural abundance of both sodium and iron. Another study reports the synthesis of $Na_2FeSiO_4$ in an impure form (85%) with $Na_2SiO_3$ as the major impurity.[14] A specific capacity of 126 mA h $g^{-1}$ has been measured in this case. Treacher and coworkers investigated the diffusion rates of a $Na_4CoSiO_4$ cathode, synthetised using a novel co-precipitation method.[19] Experimental results indicate the presence of two polymorphs, corresponding to Pc and Pbca space groups. A reversible specific capacity larger than 100 mA h $g^{-1}$ is measured. Numerical simulations, based on an empirical interatomic potential,[21] predict a very stable structure with rare occurrence of Na/Co anti-site defects, in agreement with the fist principle calculations for $Na_2FeSiO_4$.[12] In this work we investigate the configurational space of intermetallic orthosilicates by means of Density Functional theory, with the aim of exploring the possible polymorphism of these compounds (Sec. 2). We analyse a variety of structures, corresponding to different space groups and exhibiting the diamond-like structure for tetrahedral blocks which is at the base of their excellent structural stability.[12,13] This study is carried out for different transition metals $M$ = Mn, Fe, Co, Ni. In each case, the ionic ground state is found to be Pc-symmetric, in agreement with experimental observation for Mn and Co.[19,20] Results for Fe indicate a more complex polymorphism: experimental samples compatible with the Pc space group are reported in Reference[14], but more complex structures are observed in other works.[15] Our analysis is extended (Sec. 3) to the study of bonding properties and charge transfer, in order to provide a physical-chemical insight on the interactions between Na, Si, Fe and their nearest enighbours (O atoms). We thus proceed studying the average voltage of sodium deintercalation/intercalation, the respective structural change for every compound (Sec. 4). Finally, we explore the possible diffusion paths for Na in iron orthosilicates, and provide the barrier height for this process for varying transition metal atoms.

## 1 Computational Details

Total energies are calculated using the projected-augmented plane-wave (PAW) implementation of the Vienna ab initio simulation package (VASP).[22–25] Calculations are performed using the Perdew, Burke, and Ernzerhof (PBE) functional for the exchange-correlation term, with the Hubbard parameter correction (GGA+U), following the rotationally invariant form.[26,27] This approach is known to provide accurate results for lithium orthosilicates, often in line with the computationally more expensive HSE06 approach.[28] Effective $U$ values for the $d$ states of Mn, Fe, Co, Ni are chosen to be 4.0 eV, 2.7 eV, 5.0 eV and 5.1 eV. The effective on-site Exchange interaction parameter $J$ is fixed to 1 eV. These values yield to a good agreement with experimental reports in the Li case.[9] The optimised structures are obtained by minimising both the stress tensor and the Hellman-Feynman forces, using the conjugate-gradient algorithm with an energy convergence threshold of $10^{-3}$ eV.

Brillouin zone (BZ) integration is performed with Γ-centred Monkhorst-Pack grids,[29] using an electronic smearing following the Methfessel-Paxton method,[30] with a gaussian broadening of 0.2 eV. The size of the grid depends on the cell volume and on its shape. It is found that a energy convergence within 1 meV is obtained using a resolution of 0.15 $Å^{-1}$ in reciprocal space and a 500 eV kinetic energy cutoff for the plane wave expansion. For each of the considered structures, a complete geometry optimisation (cell shape and volume, atomic positions) is performed, followed by the application of a tensile/compressive diagonal strain, necessary to obtain the total energy of the system as a function of volume for a fixed cell shape. We use 3 increments in both tension and compression, each corresponding to a 1% volume update. The resulting energy profile is then fitted to the Murnaghan equation of state.[31] Both ferromagnetic (FM) and anti-ferromagnetic (AFM) calculations are carried out for the Pc-symmetric $Na_2FeSiO_4$ system. Equivalent results are obtained, with a total energy difference lower than 2 meV, well below the accuracy threshold of DFT. Moreover, the magnetic moment for a Fe atom calculated from site-projection of $d$ orbitals is found to be 3.59 $\mu_B$ in both FM and AFM cases. In the rest of the paper only results of FM calculations are presented. Our result are also tested for varying $U$ values for the Pc-symmetric $Na_2CoSiO_4$ structure. The energy-volume curves obtained for $U$ = 5.1 eV, 5.5 eV, 6.0 eV produce the same fitting parameters to the equation of state (apart from a shift in the total energies, consistent with the DFT+U approach).

The electronic density of states (DOS) and the site-project density of states (PDOS) are evaluated using the tetrahedron method with Blöchl corrections for BZ sampling.[32] This method is known to provide accurate DOS profiles, avoiding the negative occupancy resulting from the Methfessel-Paxton gaussian broadnening. The band gap values are evaluated from the so-obtained DOS as the distance on the energy axis between the maximum of the valence band and the minimum of the conduction band. It is well known that the band gap values of solids obtained from standard DFT calculations are systematically underestimated due to discontinuity in the exchange-correlation potential. These values are tipically 30-50% smaller than experimentally measured ones and exhibit a strong dependence on the approximations used for the exchange and correlation terms.[33] In the present work, due to the large number compounds involved, we have used only the GGA+U approximation. The atom-resolved charge transfer is calculated via the Bader decomposition scheme,[34] and the covalency of the bonding is discussed studying the Electron Localisation Function (ELF).[35]

The average Na-intercalation voltage is calculated as:

$$V(x_1,x_2) = \frac{E(x_2) - E(x_1) - (x_2 - x_1)\mu}{x_2 - x_1} \quad (1)$$

where $x_1, x_2$ are the number of Na atoms in the unit cell and $E(x)$ is the total energy. The chemical potential $\mu$ accounts for the different stoichiometry, and it fixed to the total energy of a bcc Na crystal. The $Na_2FeSiO_4$ system is used as a reference.[12]

The Na diffusion barrier height is calculated using the Nudged Elastic Band (NEB) method.[36,37] A supercell is used to ensure a large separation between repeated images, and five replicas of the system are created by linear interpolation between the initial and final states. A NEB calculation is then performed to obtain a guess for the minimum energy path (MEP). After convergence, the calculation is restarted, using the climb-image method to improved the estimate for the barrier.[38] The optimisation of intermediate images is always carried out using the FIRE algorithm with a force convergence threshold of 50 meV/Å.[39] The hopping distance $b$ and the activation energy $E_a$ are used to evaluate the diffusion coefficient as

$$D = d^2 \nu_0 \exp(-E_a/k_B T) \quad (2)$$

where $k_B$ is the Boltzmann constant, $T$ the temperature and $\nu_0$ the attempt frequency, assumed to be $10^{13}$ Hz.[9]

The Atomic Simulation Environment (ASE) code[40] is used for converting format of input/output files and data analysis. Ball-and-Stick and tetrahedral models are rendered using VESTA,[41] data-grids for charge density and electron localisation function are visualised with XCrySDen.[42] Plots are generated using gnuplot.[43]

## 2 Structural Stability

In this section we present the results of first-principle calculations aimed at the identification of structural minima for sodium orthosilicates. The optimal cell parameters are calculated starting from different symmetries, and the total energies are compared in order to identify the ionic ground state of the system. We focus on structures characterised by a diamond-like Fe–Si network, composed by only tetrahedral $AO_4$ ($A$ = Fe, Si) blocks, recently shown to exhibit great structural stability.[12] We investigate 12 structures pertaining to this family, exhibiting different symmetries, labelling them with the correspondent space group. This study is carried out for $Na_2MSiO_4$ orthosilicates, for $M$ = Mn, Fe, Co, Ni, following the procedure detailed in Section 1. The so-obtained structural parameters ( the total energy and the volume per formula unit, the bulk modulus and its derivative with respect to pressure) are reported in Table 1. The energy-volume curves for $Na_2FeSiO_4$ are displayed in Figure 1. Equivalent plots for $M$ = Mn, Co, Ni are reported in the ESI.

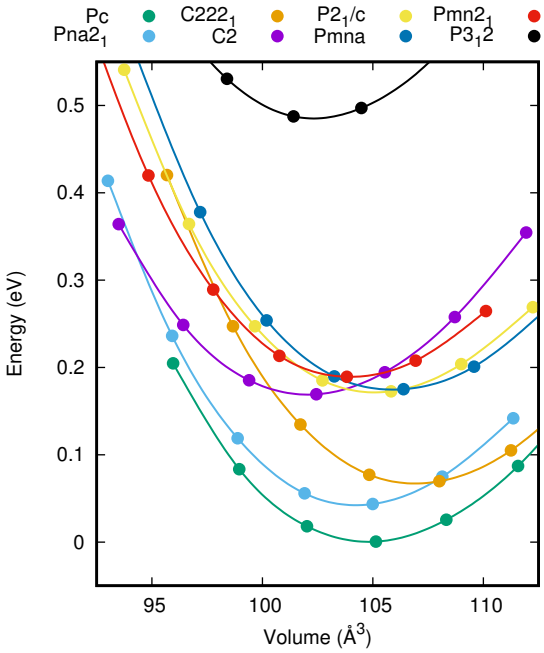


**Fig. 1** Energy-Volume curve for stable $Na_2FeSiO_4$ structural minima, labelled using the symmetry of the optimised configuration. The 0 energy is fixed to the minimum of the Pc curve.

The structural optimisation can modify the starting symmetry of the system. The Pmn2$_1$-modi and Pmn2$_1$-ncycled structures relax to similar Pc-symmetric configurations. Even though these structures are equally stable and the predicted equilibrium volume is the same, the $b/a$ and $c/a$ ratio is different. This does not influence crystal properties within the typical DFT accuracy.

**Table 1** Space group for the initial and the optimised structures and parameters of the equation of state. Volume and energies are given per formula unit. The zero value for the latter is set to the value of the most stable structure

| Symmetry | | Energy diff. (eV/f.u.) | | | | Volume (Å$^3$/f.u.) | | | | Bulk mod. (GPa) | | | | Bulk mod. derivative | | | |
|---|---|---|---|---|---|---|---|---|---|---|---|---|---|---|---|---|---|
| starting | optimised | Mn | Fe | Co | Ni | Mn | Fe | Co | Ni | Mn | Fe | Co | Ni | Mn | Fe | Co | Ni |
| Pc (7) | Pc (7) | 0.00 | 0.00 | 0.00 | 0.00 | 107.12 | 104.80 | 103.39 | 102.71 | 70.64 | 72.91 | 75.67 | 75.82 | 5.79 | 5.14 | 5.10 | 4.85 |
| $Pmn2_1$-modi | Pc (7) | 0.00 | 0.00 | 0.00 | 0.00 | 107.19 | 104.80 | 103.26 | 102.51 | 71.39 | 75.02 | 78.34 | 75.67 | 4.89 | 4.57 | 4.16 | 5.06 |
| $Pmn2_1$-ncycled | Pc (7) | 0.00 | 0.00 | 0.00 | 0.00 | 107.23 | 104.85 | 103.36 | 102.53 | 71.12 | 75.92 | 75.72 | 75.86 | 4.83 | 4.32 | 4.72 | 5.09 |
| $P2_1$n-ncycled | Pc (7) | 0.03 | 0.03 | 0.04 | 0.03 | 108.03 | 105.56 | 104.00 | 103.13 | 72.32 | 74.90 | 76.75 | 76.41 | 4.54 | 5.08 | 4.74 | 4.67 |
| $Pna2_1$ (33) | $Pna2_1$ (33) | 0.03 | 0.04 | 0.06 | 0.05 | 106.85 | 104.34 | 102.98 | 102.15 | 72.12 | 76.68 | 77.61 | 77.73 | 5.06 | 4.90 | 5.03 | 4.41 |
| $C222_1$ (20) | $C222_1$ (20) | 0.06 | 0.07 | 0.08 | 0.07 | 109.51 | 106.98 | 104.30 | 99.83 | 73.42 | 75.73 | 75.43 | 71.50 | 4.47 | 4.89 | 4.56 | 5.48 |
| C2 (5) | C2 (5) | 0.14 | 0.17 | 0.11 | 0.21 | 109.51 | 106.38 | 102.02 | 98.94 | 71.80 | 73.74 | 76.76 | 75.29 | 4.66 | 4.67 | 4.21 | 4.21 |
| $P2_1$ (4) | $P2_1/c$ (14) | 0.20 | 0.17 | 0.27 | 0.20 | 107.46 | 105.09 | 103.71 | 102.67 | 74.91 | 75.49 | 79.43 | 78.01 | 4.76 | 5.67 | 4.80 | 5.12 |
| $P2_1/c$ (14) | $P2_1/c$ (14) | 0.21 | 0.17 | 0.27 | 0.20 | 107.30 | 105.17 | 103.69 | 102.34 | 74.74 | 75.03 | 79.38 | 77.96 | 4.66 | 5.06 | 4.43 | 5.37 |
| Pnma (62) | Pnma (62) | 0.21 | 0.17 | 0.27 | 0.22 | 107.84 | 105.93 | 104.32 | 103.02 | 73.09 | 75.09 | 78.23 | 79.59 | 5.00 | 5.17 | 4.34 | 4.02 |
| $Pmn2_1$ (31) | $Pmn2_1$ (31) | 0.20 | 0.19 | 0.28 | 0.21 | 106.28 | 104.03 | 102.58 | 101.64 | 75.46 | 76.30 | 77.13 | 76.03 | 4.22 | 4.54 | 5.35 | 5.03 |
| $P3_12$ (159) | $P3_12$ (159) | 0.84 | 0.49 | 0.92 | 0.77 | 104.87 | 102.40 | 101.49 | 99.96 | 77.12 | 85.78 | 86.63 | 89.96 | 5.71 | 4.40 | 4.55 | 4.59 |

The $P2_1$n-ncycled structure relaxes to a local minimum corresponding to a Pc-symmetric configuration. Another unstable phase correspond to the $P2_1$ spaces group, which relaxes into $P2_1/c$. All the minima obtained are within an energy window of 0.3 eV from the ionic ground state Pc (with the only exception of $P3_12$, greatly unfavourable especially in the case of Mn and Co). Moreover, the calculated equilibrium volumes are very similar, indicating a great structural stability in spite of the observed polymorphism. We also note that the ordering of the energies is conserved for varying $M$, indicating that the observed structural stability would be preserved by doping of the material, relevant to battery materials e.g. for tuning the voltage. The examined structures exhibit small values for the bulk modulus (soft materials). This is the mechanical consequence of their characteristic porous structures, and phase transitions may therefore occur, even at moderate pressure. The stable configurations obtained in this work are shown in Figure 2 using coordination polyhedra.

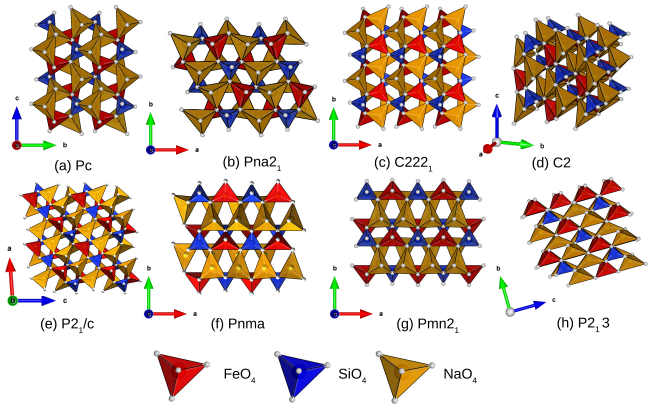


**Fig. 2** Optimised geometries for $Na_2FeSiO_4$ compounds presenting a diamond-like network. $AO_4$ groups are indicated with red, blue and yellow tetrahedra for $A$ = Fe, Si and Na respectively

Our results are consistent with literature. In Reference[19] the experimental structure of $Na_2CoSiO_4$, synthesised using both co-precipitation and solid-state synthesis, is compatible with the Pc space group. The parameters for the elementary cell, obtained from X-ray diffraction (XRD) patterns, are reported in Table 2 and compared with our simulations. A good agreement is observed, as the deviation between the experimental and the theoretical values for lattice parameters is below 2%. Notably, all the three Pc-symmetric minima found, starting from Pc, $Pmn2_1$-modi and $Pmn2_1$-ncycled, are consistent with the experimental measurement. In reference[20] $Na_2MnSiO_4$ is synthesised using the sol–gel method, and a Pc-compatible structure is obtained. The experimental data, reported in Table 2, are in agreement with our results. In the case of iron orthosilicates different experimental observations are reported in litterature. In Reference[15] XRD patterns would suggest a cubic cell with space group F$\bar{4}$3m. First-principle calculations do not predict the existence of such a structure[13], and the experimental structure is rationalised as an ensemble average of $P2_13$, $C222_1$ and C2 phases. In another experimental work[14] on $Na_2FeSiO_4$, the sample is compatible with the Pc space group. Results from this Reference are reported in Table 2 and are in excellent agreement with our calculations. Note that our prediction of stable structures exhibiting C2 and $C222_1$ symmetry (Table 1) is partially supporting the experimental observations in Reference[15].

**Table 2** Comparison between this work, experimental (exp.) data and other theoretical (theo.) calculations already present in literature. The space group and the cell parameters are reported

| source | $M$ | space group | approach | $a$ (Å) | $b$ (Å) | $c$ (Å) | $\gamma$ |
|---|---|---|---|---|---|---|---|
| this work | Co | Pc | theo. | 6.97 | 5.32 | 5.58 | 89.98 |
| this work | Co | $Pmn2_1$-modi | theo. | 7.06 | 5.29 | 5.56 | 90.15 |
| this work | Co | $Pmn2_1$-ncycled | theo. | 7.02 | 5.30 | 5.58 | 90.07 |
| Ref.[19] (i) | Co | Pc | exp. | 7.03 | 5.48 | 5.25 | 89.95 |
| Ref.[19] (ii) | Co | Pc | theo. | 7.01 | 5.47 | 5.24 | 89.88 |
| Ref.[15] | Fe | C2 | theo. | 7.47 | 7.44 | 7.45 | 90.03 |
| This work | Fe | C2 | theo. | 7.43 | 7.44 | 7.41 | 90.02 |
| Ref.[15] | Fe | $C222_1$ | theo. | 7.49 | 7.48 | 7.46 | 90.00 |
| This work | Fe | $C222_1$ | theo. | 7.91 | 8.03 | 6.77 | 90.00 |
| Ref.[15] | Fe | F$\bar{4}$3m | exp. | 7.33 | - | - | - |
| Ref.[14] | Fe | Pc | exp. | 7.16 | 5.40 | 5.69 | 89.83 |
| This work | Fe | Pc | theo. | 6.88 | 5.38 | 5.68 | 89.43 |
| This work | Fe | $Pmn2_1$-modi | theo. | 6.84 | 5.35 | 5.75 | 90.66 |
| This work | Fe | $Pmn2_1$-ncycled | theo. | 6.81 | 5.37 | 5.76 | 89.87 |
| Ref.[20] | Mn | Pc | theo. | 6.96 | 5.61 | 5.30 | 89.78 |
| Ref.[20] | Mn | Pc | exp. | 7.04 | 5.58 | 5.33 | 89.82 |
| This work | Mn | Pc | theo. | 7.02 | 5.68 | 5.38 | 89.64 |
| This work | Mn | $Pmn2_1$-modi | theo. | 7.05 | 5.70 | 5.33 | 90.21 |
| This work | Mn | $Pmn2_1$-ncycled | theo. | 7.01 | 5.73 | 5.35 | 90.29 |

The structural parameters and atomic coordinates for two degenarate Pc-symmetric minima ($M$ = Fe) are reported in Table 3.

**Table 3** Lattice parameters and atomic coordinates for the $Na_2FeSiO_4$ minima with space group Pc (7). Wyckoff positions account for multiplicity

| | Pc (Pc) | | | | Pc ($Pmn2_1$-modi) | | | | Pc ($Pmn2_1$-ncycled) | | | |
|---|---|---|---|---|---|---|---|---|---|---|---|---|
| | *a* (Å) | *b* (Å) | *c* (Å) | $\gamma$ | *a* (Å) | *b* (Å) | *c* (Å) | $\gamma$ | *b* (Å) | *c* (Å) | $\gamma$ | |
| | 6.87725 | 5.67910 | 5.38408 | 89.434 | 6.84159 | 5.75163 | 5.35012 | 90.667 | 6.84159 | 5.75163 | 5.35012 | 90.667 |
| atom | x | y | z | Wyckoff pos. | x | y | z | Wyckoff pos. | x | y | z | Wyckoff pos. |
| Fe1 | 0.25440 | 0.31754 | 0.75914 | 2*a* | 0.48209 | 0.68082 | 0.74266 | 2*a* | 0.48209 | 0.68082 | 0.74266 | 2*a* |
| Na1 | 0.49791 | 0.16173 | 0.49397 | 2*a* | -0.00274 | 0.32088 | 0.75548 | 2*a* | -0.00274 | 0.32088 | 0.75548 | 2*a* |
| Na2 | 0.74470 | 0.31961 | 0.24516 | 2*a* | 0.74733 | 0.15802 | 0.00013 | 2*a* | 0.74733 | 0.15802 | 0.00013 | 2*a* |
| O1 | 0.02494 | 0.20113 | 0.33936 | 2*a* | -0.09907 | 0.79878 | -0.02551 | 2*a* | -0.09907 | 0.79878 | -0.02551 | 2*a* |
| O2 | 0.47176 | 0.09125 | 0.89682 | 2*a* | 0.34324 | 0.08751 | 0.02648 | 2*a* | 0.34324 | 0.08751 | 0.02648 | 2*a* |
| O3 | 0.29896 | 0.66239 | 0.73369 | 2*a* | 0.16832 | 0.69928 | 0.80165 | 2*a* | 0.16832 | 0.69928 | 0.80165 | 2*a* |
| O4 | 0.19446 | 0.29968 | 0.06924 | 2*a* | 0.50908 | 0.33922 | 0.69885 | 2*a* | 0.50908 | 0.33922 | 0.69885 | 2*a* |
| Si1 | -0.00213 | 0.18806 | 0.00762 | 2*a* | 0.23333 | 0.81095 | 0.00015 | 2*a* | 0.23333 | 0.81095 | 0.00015 | 2*a* |

# 3 Chemical properties

## 3.1 Density of states and band structure

In this section we provide further insight about the elecronic properties of the Pc-symmetric $Na_2SiO_4$ compound. The total density of electronic states, calculated following the procedure described in Section 1, and the band structure along a high-symmetry path in the BZ are reported in Figure 3. The Fermi level $E_F$ is conventionally fixed to 0 eV, and separate plots are shown for the spin up and down channel, in panel (a) and (b) respectively. These channels present similar features. Very localised states are observed in the -6 eV region. Magnetic effects are not very important here, as only a small energy shift ($\sim 0.5$ eV) between the channels is observed and the shape of the peaks is very similar, indicating a low contribution from the (strongly magnetised) *d* states of the Fe atom. The region between -6 eV and the Fermi level comprise the majority of valence states, including a large contribution from the Fe *d* states. Magnetism has therefore a large impact on this area. The spin up channel exhibits several non-localised peaks, distributed between -5.5 eV and -2.3 eV. In the spin down channel instead four distinct peaks are observed. The first three are comprised between -5 eV and -3 eV, and are separated by the fourth one by a 3 eV gap. The two semi-degenerate valence bands are the only contributors to this last peak.

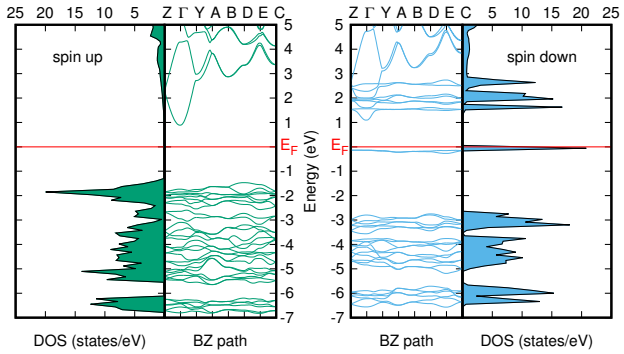


**Fig. 3** Total density of states and band structure along a high symmetric path in the BZ for the Pc-symmetric $Na_2FeSiO_4$. The data for the two spin channels (up and down) are plotted separately in panels (a) and (b) respectively. The Fermi level $E_F$ is indicated with a red line.

The unoccupied states have a different distribution between the two spin channels. Spin up electron states are not localised, and the overall contribution to the density of states is negligible. Unoccupied spin down states are instead more dense in the region comprised between 1.5 eV and 3 eV, where major *d* peaks of the DOS are observed. The minimum of the conduction band is observed at the Γ point for both spin channels. The valence band for the spin down channel is constant along the path between *Z* and Γ, where it exhibits its maximum value. The band gap can therefore be identified as a direct one at the Γ point, but indirect $Z-\Gamma$ transitions are also favourable. Another maximum of the valence band is observed at intermediate distance between E and C, lower in energy with respect to the value at Γ by less than 10 meV. The band gap for these transitions is 1.23 eV, much lower than what observed for the spin up channel (at least 2.5 eV). The presence of a small band gap (see also Table 4), qualifies this material as a semi-conductor. Note that this values is expected to underestimate experimental measurements, as discussed in Section 1. The electronic structure of $Na_2FeSiO_4$ is further analysed by calculating the site-projected density of states, displayed in Figure 4.

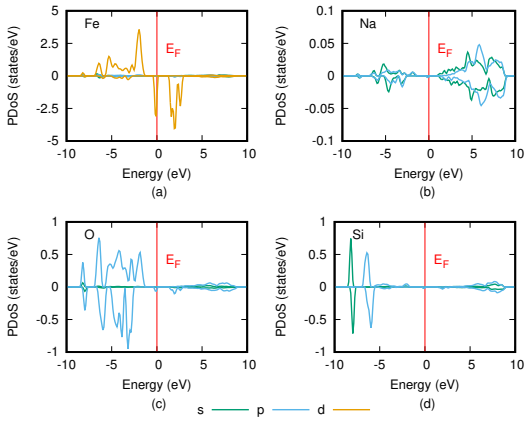


**Fig. 4** Calculated Site-projected density of state for the $Na_2FeSiO_4$ phase in Pc-symmetry. The relevant states for Fe, Na, O, Si are shown in panels (a), (b), (c) and (d) respectively. The spin down channel is conventionally plotted on the negative *y* axis. The Fermi level $E_F$ is indicated with a red line.

As previously observed, Fe *d* states, shown in panel (a), provide only a minor contribution for energy values lower than -5.5 eV. Their peaks are observed at very important energy values: -2 eV and -0.1 eV, marking the valence band of both spin up and spin down channels, and 1.5 eV marking the conduction band of the spin down channel. Given the abundance of *d* states at these values, transitions from the valence to the conduction band are more likely for these electrons, in accordance with the metallic nature of bulk Fe. Comparison between the PDOS of Fe and O, shown in Figure 4 panels (a,c), provide information about the bonding between these two atoms. A degree of covalency can be expected from the degeneracy at -2 eV between Fe *d*-electrons and O *p*-electrons, corresponding to the majority of *d* states in the spin up channel. On the other hand, the PDOS for the two elements are very different for the spin down channel due to the lack of magnetisation of the O atom. The spin up channels, apart the aforementioned peak, present also different shapes. We can therefore expect the Fe–O bonding to be prevalently non-directional, and to have an ionic character in virtue of the charge transfer expected in this material and calculated in section 3.2.

The opposite behaviour is observed for the Si–O bonds in Figure 4 panel (c,d). The two peaks observed for silicon at -8 eV (*s* states) and -5.5 eV (*p* states) are degenerate with the first two *p* states peaks of oxygen, as can be observed comparing panels (c) and (d) in Figure 4. This is a clear sign of covalent bonding. The Si atom presents also scarcity of states at the Fermi level, so that electronic transitions are very unlikely. The Na–O bonding exhibits instead a low level of covalency. While some degeneracy is present (peaks at -5.5 eV and -2 eV) the major contribution of Na to the density of states is given at -5 eV for both spin channels. A similar peak is also observed for the spin up channel of Ni, indicating a non-negligible interaction between these two atoms. This is compatible with their intertomic distance of 3.24 Å. The overall bonding of Na atoms is expected to have a Na–O ionic component and a Na–Fe interactions, probably of metallic character. Overall, directional bonding is not expected to occur, in agreement with the excellent ionic conduction properties observed in Section 4.

A full chemical characterisation of all the compound examined in Section 2 is out of the scope of this work. We limit ourself to calculate the band gap for the examined systems, reported in Table 4. The band gap is shown to have a significant dependence on the transition metal atoms. The iron-based system is characterised by a low value for the band gap, which drastically increases by a factor of 2 for stable but energetically unfavourable compounds exhibiting P21/c symmetry. The other compounds exhibit systematic larger band gap values with ordering Co>Ni>Mn, with the only exception of the aforementioned P21/c case. We note a grand stability in the magnetic moment, which conserves the reference value for the isolated atom in all the examined cases.

**Table 4** Band gap values for the examined systems, labelled according to space groups

| | Band gap (eV) | | | |
|---|---|---|---|---|
| Space group | Mn | Fe | Co | Ni |
| Pc (7) | 2.37 | 1.23 | 3.02 | 2.44 |
| $Pna2_1$ (33) | 2.31 | 1.42 | 3.07 | 2.35 |
| $C222_1$ (20) | 2.38 | 2.47 | 2.91 | 2.58 |
| C2 (5) | 2.40 | 1.31 | 3.11 | 2.22 |
| P21/c (14) | 2.30 | 2.51 | 2.82 | 2.33 |
| Pmna (62) | 2.20 | 1.54 | 2.86 | 2.22 |
| $Pmn2_1$ (31) | 2.37 | 1.47 | 2.70 | 2.25 |
| $P3_12$ (149) | 2.10 | 2.11 | 2.64 | 1.81 |

### 3.2 Charge transfer and Bonding

The study of the equilibrium Pc-symmetric phase of $Na_2FeSiO_4$ is pesently further enriched by analysing the charge redistribution in the system and by further characterising the bonding. The charge density plot is displayed in Figure 5, panels (a,d) for two different $z$ planes, containing Na, O, Si and Na, O, Fe atoms respectively. The maxima of the charge density are observed at the Fe atoms sites. This is easily understood in virtue of the number of valence electrons (8), larger with respect to the other atomic species considered (1, 4 and 6 for Na, Si and O respectively). Notably, charge peaks in correspondence of O atoms are comparable to Fe ones, indicating a charge transfer process. The Na atoms in both panels (a,d) are indistinguishable from the background, indicating charge depletion from this site. These observations are confirmed by the charge density difference, calculated with respect to a reference superposition of atomic orbitals, displayed for the same atomic planes in Figure 5 panels (c,f). Charge depletion is observed for both the Na and the Fe atoms, and it is larger in the latter case, while the O atoms are gaining a significant amount of electrons. The Bader decomposition is used to quantify this charge transfer, reported in Table 5. The Fe and Na atoms are found to be depleted, while O is gaining electron consistently to what observed in Figure 5. The larger gain of the O1 atom is explained from its short distance from the Na2 atom (2.27 Å, to be compared with the average value of 2.31 Å).

The Fe–O bond is prevalently ionic. Nevertheless, a covalent (directional) component is present, as can be appreciated from the charge transfer to the interstitial region between Fe and O observed in Figure 5 panel (c). The charge distribution around the Na atom is spherically symmetric. The Na–O bonding can be therefore identified as pure ionic. Note that the greater ionicity of Na–O with respect to Fe–O is compatible with the electronegativity difference between these atoms. In the Si–O case the interaction is mainly covalent, as can be observed from the negligible charge transfer for Si and the lack of spherical symmetry for the charge distribution pertaining to the oxygen atom.

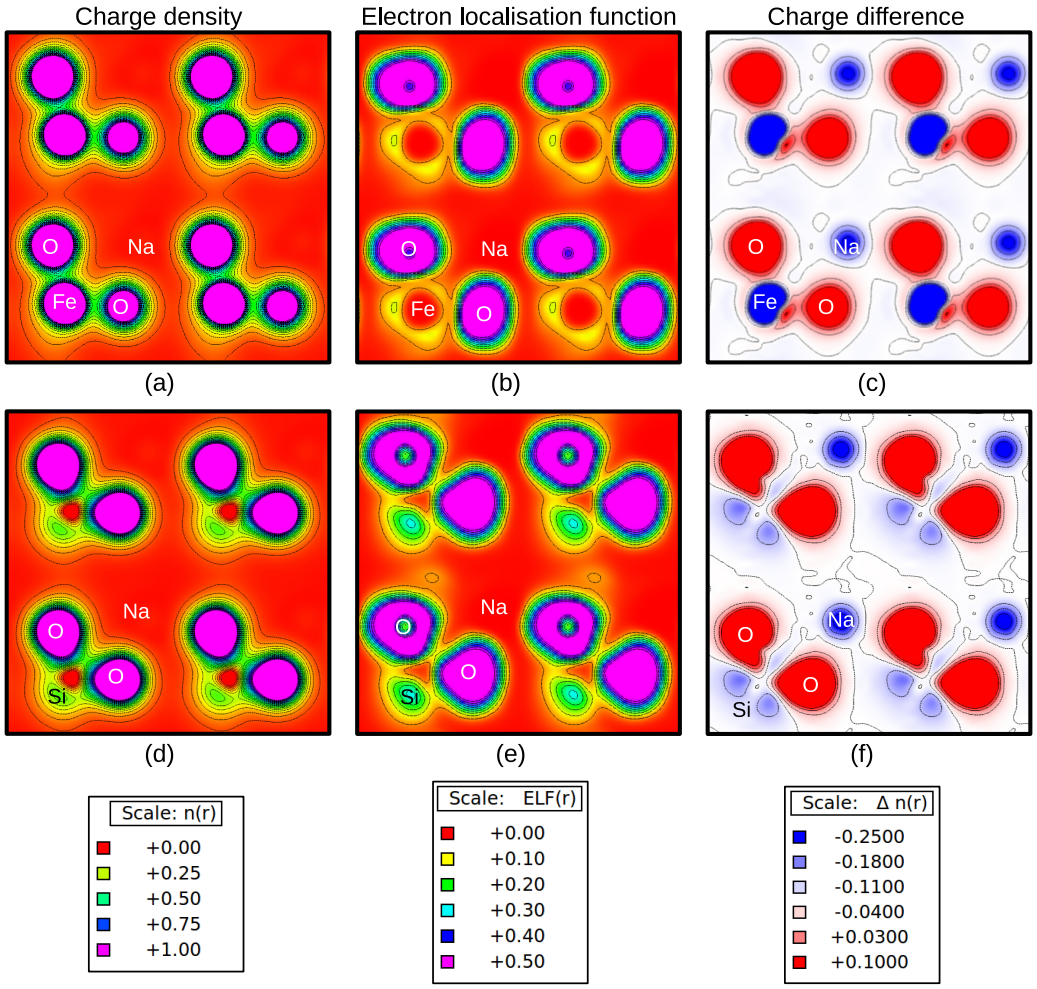


**Fig. 5** Charge density (a, d), charge difference (b, e) and electron localisation function (c, f) plots for the optimised $Na_2FeSiO_4$ Pc-symmetric phase. Two different atomic $z$ planes are shown containing respectively Fe Na O (a, b, c) and Si, Na, O (d, e, f) atoms.

A further level of analysis is provided by the electronic localisation function (ELF). In a many-electron system, the ELF, positive and smaller than 1 by construction, can be shown to have its maximum values in regions where bonding between electrons exhibits covalent nature, or for unpaired electrons (directional dangling bonds). The ELF is a constant by definition in the case of a homogeneous electron gas, this value chosen to be 0.5. Values of this order indicate the metallic character of the bonding. In this system, the ELF reaches the maximum value of 0.72, indicating the lack of pure covalent interactions. Contour plot for this quantity are shown in Figure 5 panels (b, e). The ELF exceedes the value of 0.5 only in correspondence to O atoms. This is an expected feature, given the large electronegativity of this atom. Larger values of ELF can be noticed in proximity of the Si atom, indicating a pronounced covalency. Notably, the tendency to form a covalent bond is observed also for O–O pairs. In the case of Fe atoms smaller ELF values are observed. Owing to the large charge transfer between Fe and O, a repulsive interaction between O atoms is observed, marked by the polarisation of the ELF. The contribution from the Na atom is negligible. In fact, this atom is not distinguishable from the background. This is the footprint of pure ionic bonding, and complements the observations from Section 3.1 and Figure 4.

**Table 5** Atom-resolved charge transfer for Pc-symmetric $Na_2FeSiO_4$ as evaluated by Bader decomposition. A superposition of atomic orbitals is used as a reference. The atom notation is consistent with Table 3

| atom | Fe1 | Na1 | Na2 | O1 | O2 | O3 | O4 | Si |
|---|---|---|---|---|---|---|---|---|
| charge | -1.26 | -0.44 | -0.45 | +0.65 | +0.41 | 0.51 | 0.59 | +0.00 |

## 4 Electro-chemical properties

### 4.1 Average Intercalation Potential

In the previous sections we have identified equilibrium structures having Pc symmetries for sodium orthosilicates, and we have provided a complete characterisation of the bonding between atoms. Here we analyse the consequences of these electronic properties by calculating the electro-chemical features, thus providing insight about the application of such materials as cathode for Na-ion batteries. As a first step, the volume change of these structures upon Na deintercalation is calculated. This provide crucial information about the structural stability of the material upon battery cycling. The equilibrium volumes, calculated as a function of the Na density following the structural optimisation recipe detailed in Section 1, are displayed in Figure 6. The overall volume variations are always below 4%, with the only exception of the $M = \mathrm{Mn}$ system, for which the cell is monotonically shrinking upon Na deintercalation down to a 10% variation with respect to the starting volume. In the other cases the volume of the cell is shrinking upon removal of the first Na atom per formula unit. In the fully desodiated case the volume is always within 2% from the staring value. This is in good agreement with Reference [12], for which a 2.5% decrease is observed for $NaFeSiO_4$ and no variation is found for the desodiated structure. The great structural stability of intermetallic orthosilicates is hereby verified, and only a weak dependence on the $M$ element is found, indicating that the inclusion of metallic impurities in the cathode (useful e.g. for tuning the battery voltage) would not destabilise the overall structure.

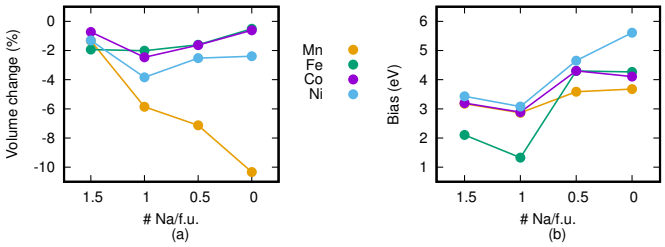


**Fig. 6** Percentage variation of equilibrium volume for desodiated structures (a) and correspondent deintercalation/intercalation voltage (b) for Pc-symmetric orthosilicates.

The total energies resulting from the volume optimisation of these systems can be used to evaluate the average voltage of sodium deintercalation/intercalation (see Equation 1). These values are displayed in Figure 6 (b). The $M = \mathrm{Fe}$ compound exhibits the lowest value of the series. This is in line with known results for Li orthosilicates, and for Na ones with $Pmn2_1$ symmetry [16]. The calculated extraction energy for the first and the second atom, respectively 2.1 eV and 4.3 eV, are in good agreement with values encountered in literature (about 2 eV/4.4 eV for $Pmn2_1$, $C222_1$ and Pc, while C2 is found to have the lower value of about 1.6 eV / 4.4 eV). [12,13,16]

### 4.2 Ionic Conductivity

The diffusion properties of Na atoms in the equilibrium Pc-symmetric phase are investigated using the NEB method, as detailed in Section 1. A $2 \times 2 \times 2$ supercell of the original structure is used, corresponding to 16 formula units and to a distance of at least 10 Å between repeated images of the vacancy. Two non-equivalent Na lattice sites can be distinguished between the supercell, as shown in Table 3. We have here considered for the $Na_2FeSiO_4$ configuration two different paths connecting two equivalent sites and passing through the other one, nearest Na atom to both the sites. This intermediate state is least energetically favoured than the starting point. The values for this total energy difference for different compounds are 0.25 eV, 0.11 eV, 0.18 eV and 0.04 for Mn, Fe, Co and Ni respectively. The initial site for the vacancy is labelled (i) in Figure 7 (a,b), the intermediate state is (ii) and the final states are (iii) and (iv) respectively. Note that these final states are both equivalent to (i). The length of each path and the respective barrier for $Na_2SiO_4$ is reported in Figure 7 (c).

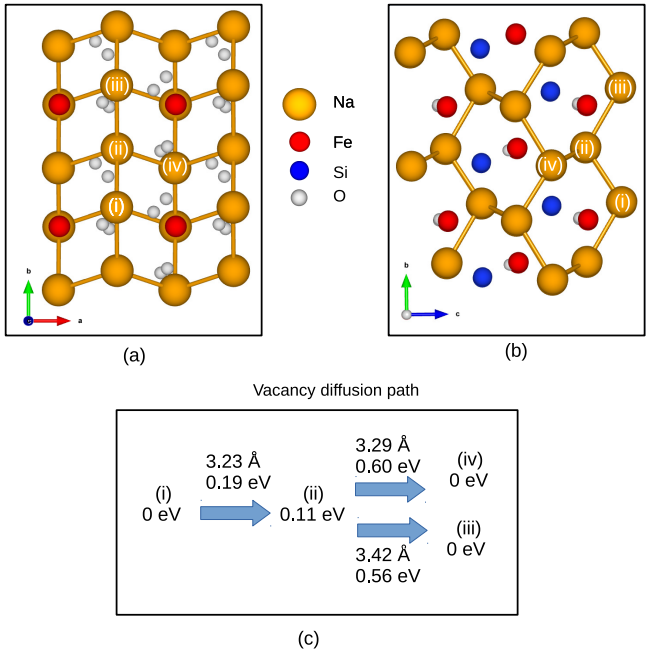


**Fig. 7** Top (a) and side (b) view of the Pc phase. Only bonds between Na atoms (yellow) are shown in order to provide a clearer view of the diffusion channels. The Fe Si and O atoms are indicated with red, blue and grey spheres respectively. The site occupied by the vacancy along the considered paths are marked with roman numbers. The bond length of single steps are shown in panel (c) for the $M = \mathrm{Fe}$ case, together with the calculated barrier heights.

**Table 6** Diffusion barrier and bond length for the MEP in $Na_2SiO_4$ compounds for $M$ = Mn, Fe, Co and Ni. The diffusion coefficients at $T = 300$ K are reported

| | path length (Å) | | | | barrier (eV) | | | | Diffusion coeff. ($cm^2\ s^{-1}$) | | | |
|---|---|---|---|---|---|---|---|---|---|---|---|---|
| path | Mn | Fe | Co | Ni | Mn | Fe | Co | Ni | Mn | Fe | Co | Ni |
| (i)→(ii) | 3.27 | 3.23 | 3.25 | 3.26 | 0.27 | 0.19 | 0.26 | 0.18 | $3.1\times10^{-8}$ | $6.7\times10^{-7}$ | $4.5\times10^{-8}$ | $1.0\times10^{-6}$ |
| (ii)→(iii) | 3.30 | 3.29 | 3.26 | 3.26 | 0.53 | 0.60 | 0.43 | 0.42 | $1.3\times10^{-12}$ | $9.0\times10^{-14}$ | $6.4\times10^{-11}$ | $9.3\times10^{-11}$ |

Notably, the minimum energy path present a very asymmetric shape, as the barrier associated to the (i)→(ii) path is significantly smaller than either the one for (ii)→(iii) or (ii)→(iv). This trend is consistent between the examined compounds, and it has been already observed for the $M$ = Mn case.[17] Given the similarity between the height of the energy barrier obtained for the cases (ii)→(iii) and (iii)→(iv) (almost the same, given the fact that the accuracy of the method is 0.1 eV), we have decided to neglect the calculation for the second path for the other compounds.

The results of NEB calculations for varying $M$ are reported in Table 6. We notice that the asymmetry between the two barriers is preserved for varying $M$. The second part of the path, indicated as (ii)→(iii) is the limiting step. Iron orthosilicate exhibits the largest barrier of the group. The overall ordering is Fe > Mn > Co ≈ Ni. Ni doping is therefore predicted to enhance the ionic conductivity of the material, without destabilising the crystal structure. This is due to the fact that the two materials have ionic ground state presenting the same symmetry, and the difference in volume between equilibrium structures is 2%, as can be noted from Table 1. Moreover, the volume change difference between Ni and Fe sodium orthosilicates upon desodiation is also within 2%.

## 5 Conclusion

The structural and electro/chemical properties of Na based orthosilicates $Na_2MSiO_4$ ($M$ = Mn, Fe, Co, Ni) are investigated by means of Density Functional Theory calculations. These compounds are characterised by a robust diamond-like $M$–Si network, which is known to provide great stability upon battery cycling. While many different phases can coexist (in a 0.3 eV energy window), the ionic ground state is shown to be Pc-symmetric for all the considered transition metal atoms $M$. The nature of the bonding is analysed by studying the density of electronic states, the charge distribution and the electron localisation function for $Na_2FeSiO_4$. Results indicate a prevalently metallic bonding between Na and surrounding atoms, partially responsible for the lowest diffusion barrier observed in the case of lithium orthosilicates. The study of electro/chemical properties reveal great cycling stabilities for Fe, Co and Ni orthosilicates (the volume change upon both partial and complete desodiation is below 5%), while Mn is under-performing, with volume change up to 10% upon complete desodiation. The calculated second Na deintercalation plateaus are lower than the respective values for Ni materials, indicating better possibilities for the extraction of two ions per formula unit, hardly achieved in the case of Li-based orthosilicates. The $Na_2SiO_4$ compound is the most relevant from a commercial perspective, due to the abundance of both sodium and iron. This material is characterised by a low voltage (for the extraction of the first ion per formula unit) and by a smaller ionic conductivity with respect to the other compounds analysed in this work. This can be addressed by Ni-doping, which is predicted to both increase the voltage and decrease the diffusion barrier for a Na vacancy, without disrupting the excellent structural stability upon cycling of the material.

## Aknowledgements

The authors gratefully acknowledge the Research Council of Norway (Grant agreement no.: Nano-MILIB, 143732; SELiNaB-255441) for financial support and for providing the computer time (under the project number NN2875k) at the Norwegian supercomputer facility.

## References

1 C. W. Mason, I. Gocheva, H. E. Hoster and D. Y. W. Yu, *Chem. Commun.*, 2014, **50**, 2249–51.
2 S. M. Wood, C. Eames, E. Kendrick and M. S. Islam, *J. Phys. Chem. C*, 2015, **119**, 15935–15941.
3 A. Rudola, K. Saravanan, C. W. Mason and P. Balaya, *J. Mater. Chem. A*, 2013, **1**, 2653–2662.
4 A. Nyte, A. Abouimrane, M. Armand and J. O. Thomas, *Electrochem. Commun.*, 2005, **7**, 156–160.
5 R. Dominko, M. Bele, M. Gabers, J. Jamnik, A. Meden and M. Rems, *Electrochem. Commun.*, 2006, **8**, 217–222.
6 J. O. Thomas, P. Larsson, R. Ahuja and A. Nyte, *Electrochem. commun.*, 2006, **8**, 797–800.
7 M. S. Islam, R. Dominko, C. S. Christian Masquelier, A. R. Armstrong and P. G. Bruced, *J. Mater. Chem*, 2011, **21**, 9811–9818.
8 D. Rangappa, K. D. Murukanahally, T. Tomai, A. Unemoto and I. Honma, *Nano Lett.*, 2012, **12**, 1146–1151.
9 P. Vajeeston and H. Fjellvåg, *arXiv:1611.04350*, 2016.
10 A. Boulineau, C. Sirisopanaporn, R. Dominko, A. R. Armstrong, P. G. Bruce and C. Masquelier, *Dalton Trans.*, 2010, **39**, 6310–6316.
11 C. Y. Chen, K. Matsumoto, T. Nohira and R. Hagiwara, *Electrochem. commun.*, 2014, **45**, 63–66.

12 P. Wu, S. Q. Wu, X. Lv, X. Zhao, Z. Ye, Z. Lin, C. Z. Wang and K. M. Ho, *Phys. Chem. Chem. Phys.*, 2016, **18**, 23916–23922.
13 Z. Ye, X. Zhao, S. Li, S. Wu, P. Wu, M. C. Nguyen, J. Guo, J. Mi, Z. Gong, Z. Z. Zhu, Y. Yang, C. Z. Wang and K. M. Ho, *Electrochim. Acta*, 2016, **212**, 934–940.
14 Y. Kee, N. Dimov, A. Staykov and S. Okada, *Mater. Chem. Phys.*, 2016, **171**, 45–49.
15 S. Li, J. Guo, Z. Ye, X. Zhao, S. Wu, J. X. Mi, C. Z. Wang, Z. Gong, M. J. McDonald, Z. Zhu, K. M. Ho and Y. Yang, *ACS Appl. Mater. Interfaces*, 2016, **8**, 17233–17238.
16 Y. Li, W. Sun, J. Liang, H. Sun, I. Di Marco, L. Ni, S. Tang and J. Zhang, *J. Mater. Chem. A*, 2016, **4**, 17455–17463.
17 P. Zhang, Y. Xu, F. Zheng, S. Q. Wu, Y. Yang and Z.-z. Zhu, *Cryst. Eng. Comm.*, 2015, **17**, 2123–2128.
18 S. Gao, J. Zhao, Y. Zhao, Y. Wu, X. Zhang, L. Wang, X. Liu, Y. Rui and J. Xu, *Mater. Lett.*, 2015, **158**, 300–303.
19 J. C. Treacher, S. M. Wood, M. S. Islam and E. Kendrick, *Phys. Chem. Chem. Phys.*, 2016, **18**, 32744–32752.
20 H. Duncan, a. Kondamreddy, P. H. J. Mercier, Y. Le Page, Y. Abu-Lebdeh, M. Couillard, P. S. Whitfield and I. J. Davidson, *Chem. Mater.*, 2011, **23**, 5446–5456.
21 A. Pedone, G. Malavasi, M. C. Menziani, a. N. Cormack and U. Segre, *J. Phys. Chem. B*, 2006, **110**, 11780–11795.
22 G. Kresse and J. Hafner, *Phys. Rev. B*, 1993, **47**, 558–561.
23 G. Kresse and J. Furthmüller, *Comput. Mater. Sci.*, 1996, **6**, 15–50.
24 G. Kresse and J. Furthmüller, *Phys. Rev. B*, 1996, **54**, 11169–11186.
25 G. Kresse and D. Joubert, *Phys. Rev. B*, 1999, **59**, 1758–1775.
26 J. P. Perdew, K. Burke and M. Ernzerhof, *Phys. Rev. Lett.*, 1996, **77**, 3865–3868.
27 A. I. Liechtenstein, V. I. Anisimov and J. Zaanen, *Phys. Rev. B*, 1995, **52**, R5467–R5470.
28 R. C. Longo, K. Xiong, W. Wang and K. Cho, *Electrochim. Acta*, 2012, **80**, 84–89.
29 H. J. Monkhorst and J. D. Pack, *Phys. Rev. B*, 1976, **13**, 5188–5192.
30 M. Methfessel and A. T. Paxton, *Phys. Rev. B*, 1989, **40**, 3616–3621.
31 F. D. Murnaghan, *Proc. Natl. Acad. Sci.*, 1944, **30**, 244–247.
32 P. E. Blöchl, O. Jepsen and O. K. Andersen, *Phys. Rev. B*, 1994, **49**, 16223–16233.
33 S. Lundqvist and N. H. March, *Theory of the Inhomogeneous Electron Gas*, Spinger US, 1983.
34 G. Henkelman, A. Arnaldsson and H. Jónsson, *Comput. Mater. Sci.*, 2006, **36**, 354–360.
35 A. Savin, O. Jepsen, J. Flad, O. K. Andersen, H. Preuss and H. G. von Schnering, *Angew. Chem. Int. Ed*, 1992, **31**, 187–188.
36 H. Jónsson, G. Mills and K. W. Jacobsen, in *Nudged elastic band method for finding minimum energy paths of transition*, World Scientific, 1998, ch. 16, pp. 385–404.
37 G. Henkelman and H. Jónsson, *J. Chem. Phys.*, 2000, **113**, 9978–9985.
38 G. Henkelman, B. P. Uberuaga and H. Jónsson, *J. Chem. Phys.*, 2000, **113**, 9901–9904.
39 E. Bitzek, P. Koskinen, F. Gähler, M. Moseler and P. Gumbsch, *Phys. Rev. Lett.*, 2006, **97**, 170–201.
40 S. R. Bahn and K. W. Jacobsen, *Comput. Sci. Eng.*, 2002, **4**, 56–66.
41 K. Momma and F. Izumi, *J. Appl. Crystallogr.*, 2008, **41**, 653–658.
42 A. Kokalj, *J. Mol. Graph. Model.*, 1999, **17**, 176–179.
43 T. Williams and C. K. et.al, *Gnuplot 4.6: an interactive plotting program*, 2013.

# A first-principle study of $NaMPO_4$ ($M$ = Mn, Fe, Co, Ni) possible novel structures as cathode materials for sodium-ion batteries: structural and electrochemical characterisation. Electronic Supplementary Information (ESI)

F. Bianchini,* H. Fjellvåg, and P. Vajeeston†

*Department of Chemistry*

*University of Oslo, Box 1033 Blindern,*

*N-0315 Oslo, Norway*

(Dated: August 24, 2017)

* federico.bianchini@smn.uio.no

† http://folk.uio.no/ponniahv

## I. STARTING DATABASE

In this section we report the initial set of 30 structures used to firstly explore the configurational space of Na iron phosphates. Only the configurations close in energy to maricite (within a 0.4 eV window) are analysed in the main text. The full initial set is provided in Table I and in Table II, indicating each structure with the correspondent ICSD Collection Code and with the original chemical composition. The space group (name and number) are also provided for each configuration for the sake of clarity, together with the energy difference (per formula unit) with respect to maricite. Note that some of these structures (e.g. ICSD collection code 82752) have been included twice in the dataset. This is due to the fact the maricite and tryphilite are related to each other by a swap of crystal sites between the Na and the Fe ions, and both maricite-like and tryphilite-like structures have been examined here for relevant octahedral coordination of the Fe atom. The structures presenting this inversion of ion sites are indicated with a $^i$ symbol after the ICSD Collection Code in Tables I, II. A discussion about the energy ordering of the structures for Na$M$PO$_4$ ($M$ = Mn, Fe, Co and Ni) is presented in the main text.

TABLE I. Entries of the ICSD databased analysed for this study. The space group and the original formula of the compound are reported for clarity. The total energy difference per formula unit with respect to maricite is indicated. The suffice $i$ indicates inversion of the original lattice sites for Fe and Na, in order to change to maricite-like to tryphilite-like geometries. The second part of the table can be found in the next page.

| ICSD | composition | space group | Energy (eV) |
|---|---|---|---|
| 10472 | $BaCdSnS_4$ | Fdd2 (No 43) | 0.44 |
| 50950 | $LiZnPO_4$ | Cc (No 9) | 0.28 |
| 237852 | $NaFePO_4$ | Pmna (No 62) | 0.00 |
| 280175 | $CoNaPO_4$ | $P2_1/c$ (No 14) | -0.01 |
| 15836 | $LiCuVO_4$ | Imma (No 74) | 3.56 |
| 72484 | $CaMgNiH_4$ | $P2_13$ (No 198) | 1.09 |
| 14048 | $NaCdPO_4$ | $Pna2_1$ (No 33) | 0.00 |
| 50457 | $TlCuPO_4$ | C2/c (No 15) | 0.43 |

TABLE II. Entries of the ICSD databased analysed for this study. The space group and the original formula of the compound are reported for clarity. The total energy difference per formula unit with respect to maricite is indicated. The suffice $i$ indicates inversion of the original lattice sites for Fe and Na, in order to change to maricite-like to tryphilite-like geometries.

| ICSD | composition | space group | Energy (eV) |
|---|---|---|---|
| 28106 | $LiBGeO_4$ | Fmm2 (No 42) | 0.68 |
| 85671 | $FeNaPO_4$ | Pnma (No 62) | 0.00 |
| 82752 | $FeNaPO_4$ | Pnma (No 62) | 0.00 |
| $82752^i$ | $FeNaPO_4$ | Pnma (No 62) | 0.25 |
| 86792 | $BaBeSiO_4$ | Cm (No 8) | 0.59 |
| 27647 | $CaAlBO_4$ | Ccc2 (No 37) | 0.23 |
| 186517 | $LiFeSiO_4$ | P1 (No 1) | 0.29 |
| 14364 | $LiNaSO_4$ | P31c (No 159) | 0.21 |
| 603205 | $KYbSiS_4$ | $P2_1$ (No 4) | 0.55 |
| 263111 | $CdBi2O_4$ | $I4_1/amd$ (No 141) | 1.04 |
| 28107 | $SrBAlO_4$ | Pccn (No 56) | 2.98 |
| 2929 | $LiAlSiO_4$ | $P6_422$ (No 181) | 0.66 |
| 97767 | $FeLiPO_4$ | Cmcm (No 63) | 0.04 |
| $97767^i$ | $FeLiPO_4$ | Cmcm (No 63) | 0.32 |
| 35451 | $BaNdGaO_4$ | $P2_12_12$ (No 19) | 0.01 |
| 30886 | $KCuPO_4$ | Pbca (No 61) | 0.15 |
| 9271 | $NaBePO_4$ | $P2_1/c$ (No 14) | 0.42 |
| 84709 | $NaCoPO_4$ | $P2_1/c$ (No 14) | 0.11 |
| 82753 | $NaCoPO_4$ | $P6_5$ (No 170) | 0.08 |
| 415458 | $KFePO_4$ | $P2_1/c$ (No 14) | 0.15 |
| 56291 | $LiFePO_4$ | Pnma (No 62) | 0.00 |
| $56291^i$ | $LiFePO_4$ | Pnma (No 62) | 0.00 |

## II. ENERGY-VOLUME CURVES

We present here the energy-colume curves for Na$M$PO$_4$ ($M$ = Mn, Ni), excluded from the main text due to the strong similarities with case of $M$ = Fe. With respect to this aforementioned case, we observe a larger energy spreading between favourable and unfavourable structures. Tryphilite is observed to be particularly favourable in the case of Mn, consistent with the existence of natrophilite, a structure which exhibits 50% occupation of the inequivalent cation sites by both Na and Mn. In the case of Co a Fe-like behaviour is observed, with a greater preference for low-volume structures. This is the only case for which the phase labelled as 'tetra 14' is least favourable than the semi-amorphous 'tetra/bp 170'. This particular tetrahedral structure is nevertheless the most favourable with respect to the other examined cases presenting the same kind of coordination for the Fe atom. Overall, these compounds are less likely to exhibit polymorphism than NaFePO$_4$, being limited to maricite and tryphilite structures. The behaviour of Co based phosphates, examined in the main text and matching relevant experimental measurements, is singular within the series as the blue, the tetraheral and the red phases are observed, and tryphilite is not.

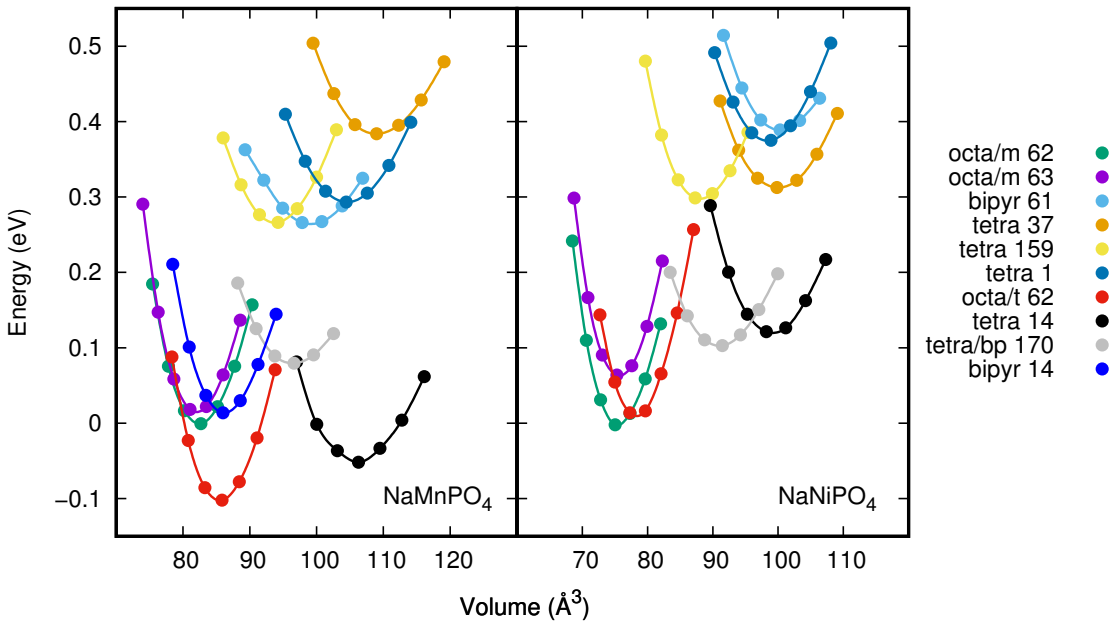


FIG. 1. Energy-volume curves per formula unit for the most energetically favourable configurations for Na$M$PO$_4$ ($M$ = Mn, Ni) compounds. Energies (per formula unit) are reported using maricite as a reference. Structures are labelled according to the coordination of the $M$ atom, octahedral ('octa'), tetrahedral ('tetra') trigonal bipyramidal ('bypir') or a mixture of the last two ('tetra/bp').

## III. NOVEL STRUCTURES

We report here the equilibrium coordinates for the two energetically most favourable novel structures for $NaFePO_4$. The structure labelled as 'tetra 14' is reported in Table III, and 'tetra/bp 170' in Table IV. The equilibrium volumes and the lattice parameters are reported in the main text, in respectively table MT-I and MT-II. The crystal symmetries of these systems are studied using the FINDSYM code, as referenced in the main text. The Wyckoff positions and the respective multiplicity are thus obtained and reported in Tables III, IV. The parameters for the structural optimisation of these structures are reported in Section II in the main text.

TABLE III. Equilibrium energy and volumes per formula unit as obtained from fitting to the Murnaghan equation of state for the analysed $NaMSiO_4$ ($M$ = Mn, Fe, Co, Mn) modifications.

| Z | Wyckoff positions | | $x$ | $y$ | $z$ |
|---|---|---|---|---|---|
| Fe1 | 4 | e | 0.71997 | 0.34186 | 0.51712 |
| Na1 | 4 | e | 0.22941 | 0.37052 | 0.01704 |
| O1 | 4 | e | 0.04999 | -0.03876 | 0.77051 |
| O2 | 4 | e | 0.88109 | 0.33934 | 0.08923 |
| O3 | 4 | e | 0.72136 | 0.67011 | 0.55922 |
| O4 | 4 | e | 0.28696 | 0.62190 | 0.70455 |
| P1 | 4 | e | -0.01592 | 0.10348 | 0.77717 |

TABLE IV. Atomic coordinates for the semi-amourphous 'tetra/bp' $NaFePO_4$ structure.

| Z | Wyckoff positions | | $x$ | $y$ | $z$ |
|---|---|---|---|---|---|
| Fe1 | 6 | a | 0.61115 | 0.82444 | 0.70964 |
| Fe2 | 6 | a | 0.32662 | 0.65734 | 0.47971 |
| Fe3 | 6 | a | 0.69396 | 0.86270 | 0.01823 |
| Fe4 | 6 | a | 0.18700 | 0.88830 | 0.01155 |
| Na1 | 6 | a | 0.06372 | 0.04718 | 0.09337 |
| Na2 | 6 | a | 0.50063 | -0.07221 | 0.24482 |
| Na3 | 6 | a | 0.48756 | 0.45171 | 0.75409 |
| Na4 | 6 | a | 0.53702 | 0.04931 | 0.08936 |
| O1 | 6 | a | 0.55966 | 0.22676 | 0.15354 |
| O2 | 6 | a | -0.01316 | 0.79543 | 0.35206 |
| O3 | 6 | a | -0.00708 | 0.32075 | 0.04766 |
| O4 | 6 | a | 0.75871 | 0.08438 | 0.25785 |
| O5 | 6 | a | 0.64794 | 0.48636 | 0.85052 |
| O6 | 6 | a | 0.07229 | 0.72902 | 0.14054 |
| O7 | 6 | a | 0.59881 | -0.08825 | 0.78246 |
| O8 | 6 | a | 0.76940 | 0.26289 | 0.47704 |
| O9 | 6 | a | 0.14424 | -0.02721 | 0.84606 |
| O10 | 6 | a | 0.29220 | 0.25519 | -0.07872 |
| O11 | 6 | a | 0.85851 | 0.06931 | -0.00339 |
| O12 | 6 | a | 0.35917 | 0.61369 | 0.73735 |
| O13 | 6 | a | 0.19222 | 0.45538 | 0.51582 |
| O14 | 6 | a | 0.51352 | 0.71795 | 0.85838 |
| O15 | 6 | a | 0.71534 | 0.70992 | -0.02941 |
| O16 | 6 | a | 0.51626 | 0.64918 | 0.49817 |
| P1 | 6 | a | 0.14806 | 0.31193 | 0.48102 |
| P2 | 6 | a | 0.63450 | 0.32997 | 0.84626 |
| P3 | 6 | a | 0.12973 | 0.77558 | 0.50502 |
| P4 | 6 | a | 0.21683 | 0.88450 | 0.14520 |

## IV. BULK MODULUS OF THE EXAMINED STRUCTURES

We report here the bulk modulus and its derivative with respect to pressure for the examined structures, as obtained from fitting to the Murnaghan equation of state of energy-volumes curves, as specified in Section II in the main text. The values obtained for the 12 most favourable configurations for varying $M$ = Mn, Fe, Co and Ni, are reported in Table V, and complement the information presented in the main text (Table MT-I).

Similarly to what observed for the equilibrium volume, the bulk modulus of these structures is correlated to the coordination of the $M$ atom. The values reported for the octahedral phases (maricite, tryphilite and related structures) are significantly larger than what observed for expanded volume configurations. These values range from 80 to 100 GPa, following the ordering Ni > Co > Fe ≈ Mn and ehxibiting a negligible difference between triphylite and maricite.

TABLE V. Atomic coordinates for the semi-amorphous 'tetra/bp' structures.

| sp. gr. | coor. | Mn | | Fe | | Co | | Ni | |
|---|---|---|---|---|---|---|---|---|---|
| | | $B$ (GPa) | $B'$ | $B$ (GPa) | $B'$ | $B$ (GPa) | $B'$ | $B$ (GPa) | $B'$ |
| 62 | octa/m | 81.34 | 5.80 | 80.87 | 5.43 | 86.38 | 6.23 | 92.80 | 6.29 |
| 62 | octa/t | 83.46 | 4.91 | 81.24 | 5.52 | 87.94 | 4.44 | 96.85 | 5.14 |
| 33 | octa/t | 83.79 | 4.75 | 88.11 | 4.41 | 88.41 | 4.70 | 97.79 | 4.30 |
| 19 | octa/t | 82.32 | 4.65 | 86.00 | 4.24 | 87.24 | 4.12 | 97.28 | 4.25 |
| 63 | octa/m | 88.36 | 5.32 | 85.57 | 5.56 | 92.28 | 4.99 | 98.73 | 4.99 |
| 170 | tetra/bp | 38.80 | 5.16 | 39.01 | 6.95 | 44.48 | 6.57 | 41.88 | 5.26 |
| 14 | bipyr | 72.28 | 6.32 | 71.69 | 6.21 | 81.70 | 6.44 | 89.42 | 6.04 |
| 61 | bipyr | 22.85 | 5.30 | 36.51 | 4.35 | 38.88 | 1.99 | 43.12 | 4.54 |
| 159 | tetra | 49.23 | 2.51 | 54.59 | 5.19 | 59.20 | 6.29 | 56.44 | 6.34 |
| 14 | tetra | 45.03 | 6.95 | 44.15 | 2.93 | 44.89 | 3.34 | 51.26 | 3.88 |
| 37 | octa | 38.68 | 4.47 | 43.66 | 3.76 | 46.81 | 6.09 | 42.20 | 2.96 |
| 1 | tetra | 41.85 | 1.53 | 47.11 | 2.25 | 45.47 | 2.83 | 49.17 | 3.01 |

The symmetric bipyramidal structure 'bypir 14' exhibits smaller values for the bulk modulus, ranging from 70 GPa to 90 GPa and following the previously described ordering across the series. The distorted bipyramidal structure 'bypir 61' exhibits the smaller values for the bulk modulus for Mn, Fe and Co. In the case of the tetrahedral phase, the reported values for the bulk modulus range from 35 GPa to 55 GPa, being therefore smaller by a factor of two than the findings for the octahedral structures. A clear ordering of the values across the series can not be observed. The semi-amorphous 'tetra/bp 170' structure exhibits a similar behaviour.